



Cyclic analysis of steel plate shear walls with coupling

M. Wang ⁽¹⁾, D.J. Borello ⁽²⁾, L.A. Fahnestock ⁽³⁾

⁽¹⁾ Associate Professor, School of Civil Engineering, Beijing Jiaotong University, Beijing, 100044, China, wangmeng1117@gmail.com

⁽²⁾ Assistant Professor, School of Civil & Construction Engineering, Oregon State University, Corvallis, OR, 97331, U.S.A.,

Daniel.Borello@oregonstate.edu

⁽³⁾ Associate Professor, Department of Civil and Environmental Engineering, University of Illinois at Urbana-Champaign, Urbana, IL, 61801, U.S.A., fhnstck@illinois.edu

Abstract

Recent large-scale cyclic tests demonstrated the viability of the Steel Plate Shear Wall with Coupling (SPSW-WC) configuration as a seismic force-resisting system for high seismic regions. These test specimens were three-story coupled walls that represented the bottom portion of a six-story prototype frame, and a hybrid simulation protocol was employed to impose demands consistent with the upper portion of the frame that was not part of the physical substructure. The research described in this paper developed three-dimensional finite element models that were validated against the large-scale tests. The models were then used to study the performance of the SPSW-WC test specimens and extend the behavioral insight by considering response quantities that could not be measured in tests. The numerical modeling approach was then used to establish full six-story reduced-scale models that verified the equivalence and accuracy of the boundary conditions for the test specimens. In addition, the performances of the reduced-scale six-story models, three-story models and experimental specimens were further compared. These results showed that the numerical simulations not only captured the global behaviors and local limit states observed in tests, but also revealed valuable new information that could not be directly obtained from the tests. The developed modeling framework provides a valuable tool for supplementing experimental data and carrying out further parametric studies of a range of SPSW-WC configurations.

Keywords: Steel plate shear wall with coupling (SPSW-WC); numerical simulation; degree of coupling (DC); cyclic pushover analysis; large-scale testing.

1. Introduction

The Steel Plate Shear Wall (SPSW) seismic force-resisting system (SFRS) has been used in a wide range of buildings, from low-rise single-family residential to high-rise mixed-use applications [1-2] due to its combination of strength, stiffness, ductility and energy dissipation capacity [3]. The Steel Plate Shear Wall with Coupling (SPSW-WC) system is a relatively new configuration of the conventional SPSW system that provides greater architectural flexibility and material efficiency, along with increased energy dissipation [4]. A typical SPSW-WC system is composed of a pair of SPSW piers connected by coupling beams (CBs) at the floor levels. Each SPSW pier consists of Horizontal Boundary Elements (HBEs), Vertical Boundary Elements (VBEs) and thin infill plates, as shown in Fig. 1.

To investigate the behavior of the SPSW-WC configuration, several researchers have carried out numerical simulations and large-scale tests. At the National Center for Research on Earthquake Engineering in Taiwan, Li et al. [5] tested a two-story reduced-scale SPSW-WC substructure of a six-story prototype office building under cyclic loading. Similarly, at the University of Illinois, the second and third authors of the present paper tested two 0.43-scale specimens that represented the bottom three stories of six-story prototype structures subjected to cyclic loading, with the boundary conditions more realistically simulated [4, 6]. Dubina et al. [7] conducted monotonic and cyclic tests on four half-scale SPSW-WC specimens with different types of HBE-to-VBE connections. All of the testing data have revealed robust cyclic behavior of SPSW-WC. However, due to the high cost of experimental testing, comprehensive evaluation of a broad range of parameters is difficult. Additionally, important internal behaviors, such as member forces and localized strains and stresses, are difficult to experimentally measure. Therefore, it is necessary to develop an accurate three-dimensional finite element model of SPSW-WC systems for supplementing experimental data and conducting parametric analyses.

In this paper, three-dimensional finite element models were developed and validated against the large-scale tests of SPSW-WC specimens conducted by Borello et al. [6]. The global behavior, failure mechanisms, and fracture locations were compared. In addition, several important indexes of the two specimens were also investigated (e.g. pier internal forces, degree of coupling and failure of VBE base). Then, based on this modeling method, the lab specimen was extended to a reduced-scale model as shown in Fig. 1, and the extended six-story reduced-scale models were used to examine the equivalence and accuracy of the hybrid simulation protocol imposed on the test specimens. Finally, the performances of the reduced-scale six-story models, three-story models and experimental specimens were further compared.

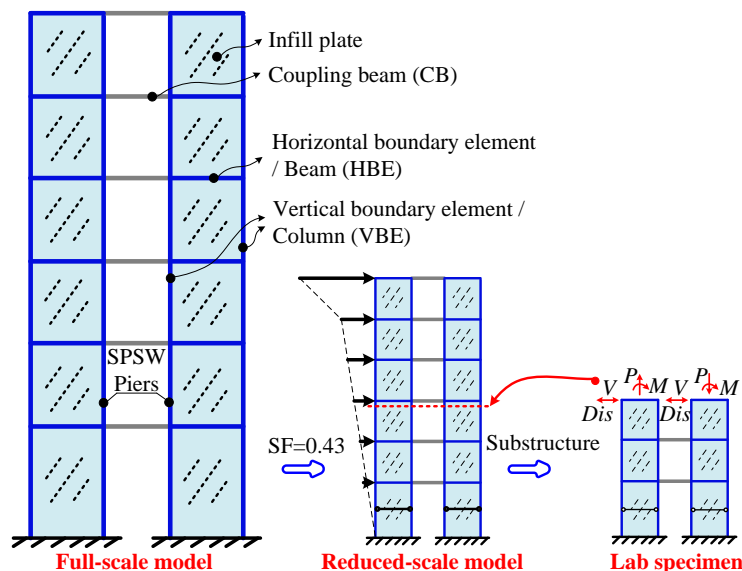


Fig.1 Relationship between SPSW-WC models.

2. Summary of reference experimental program

An experimental program [4, 6] was conducted to study SPSW-WC seismic behavior. Two test specimens (FLEX_{3s} and INT_{3s}) were designed to represent the bottom three stories of a six-story reduced-scale (Scale Factor = 0.43) model (as shown in Fig. 1). The test specimens were primarily distinguished by coupling behavior. FLEX_{3s} had flexural yielding dominated CBs, whose sizes were the same as the HBEs at corresponding stories. INT_{3s} had a higher Degree of Coupling (DC) and intermediate flexural/shear yielding dominated CBs, which had twice the plastic moment capacity of the HBEs at the same story. The infill plates were ASTM A1008 steel and the boundary members were ASTM A992 steel. The dimensions of the specimens are shown in Fig. 2. Restrainers were provided for the first floor to prevent the development of a plastic hinge above the base of the VBEs [5]. Reduced beam section (RBS) connections were used at the HBE-to-VBE interfaces. The panel zone regions of the internal VBEs were reinforced with doubler plates. The CBs were attached to the VBEs with extended end plate connections [8]. Transverse stiffeners were added to one side of the coupling beams and web reinforcements were added at the ends of the CBs to prevent plastic hinges from forming near the welds.

The specimens were tested in the MUST-SIM facility at the University of Illinois at Urbana-Champaign, shown in Fig. 3. Load and Boundary Condition Boxes (LBCBs) were used for imposing demands on the specimens that were consistent with the full six-story structure subjected to a lateral load profile (Fig. 1). The test specimens were braced out-of-plane near the floor levels. More details related to the loading protocol, test setup and the specimen designs can be found in Borello [4].

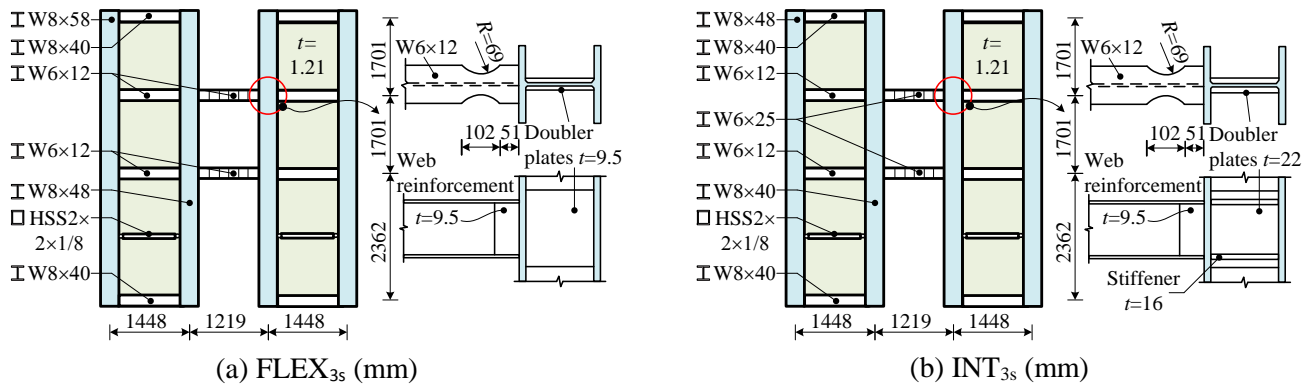


Fig.2 Specimen elevation (mm)

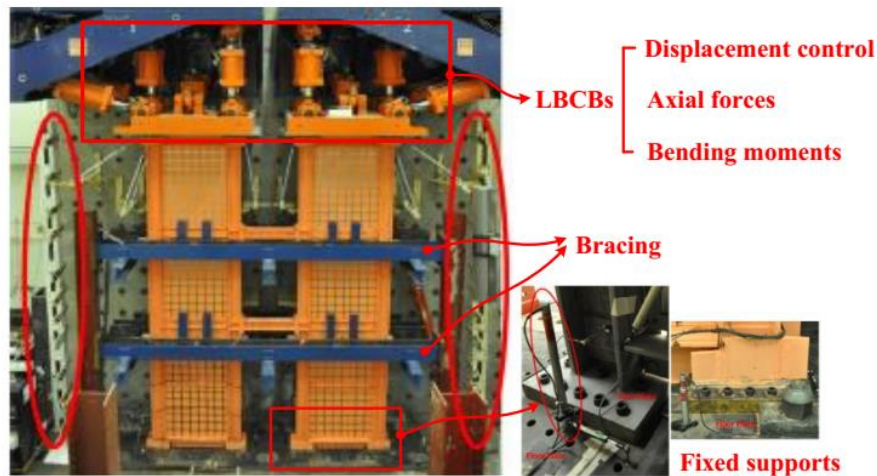


Fig.3 Experimental setup

3. Numerical simulations of experimental specimens

3.1 Description of numerical model

Three-dimension models of the SPSW-WC test specimens were developed using ABAQUS [9], as shown in Fig. 4. The boundary frame, coupling beams and infill plates were modeled with reduced-integration 4-node shell elements (S4R). Because the CB end plates were thick, their local deformations were negligible with limited influence on the global hysteretic behavior. Therefore, the coupling beams were tied to the internal VBEs directly. The measured material properties were used for the material constitutive model with combined isotropic and kinematic hardening behavior.

The interaction between the floor 1 restrainer and the infill plate is summarized in Fig. 4. Each end of the restrainer was coupled to one node of the VBE flange. Hard contact and Coulomb friction was used to model the normal and tangential contact, respectively between the restrainers and infill plate. Node-to-node coupling was used to represent the bolts sandwiching the infill plate. The boundary conditions and loading patterns were consistent with the experimental setup (Fig. 3 and Fig. 4). The bottom nodes were fixed to simulate the base connections. The out-of-plane deformations of the HBE-to-VBE connections were restrained like the experiments to avoid global instability. A constant gravity load was applied at the top of the substructure to simulate the top three stories of the six-story model. Subsequently, cyclic horizontal displacements, Δ , were imposed. The vertical force and moment at the top of each pier were then applied, proportional to the imposed horizontal force.

The specimens experienced significant nonlinear behavior such as buckling and yielding of the infill plates and flexural and shear yielding in the coupling beams and boundary elements. ABAQUS 6.10/Explicit was used, which solved the static loading as a transient analysis using the central difference integration method. The loading procedure of (Dynamic, Explicit) is set relatively slow to capture static characteristics and minimize the inertial effect. The time step was determined using the minimum mesh size of the models.

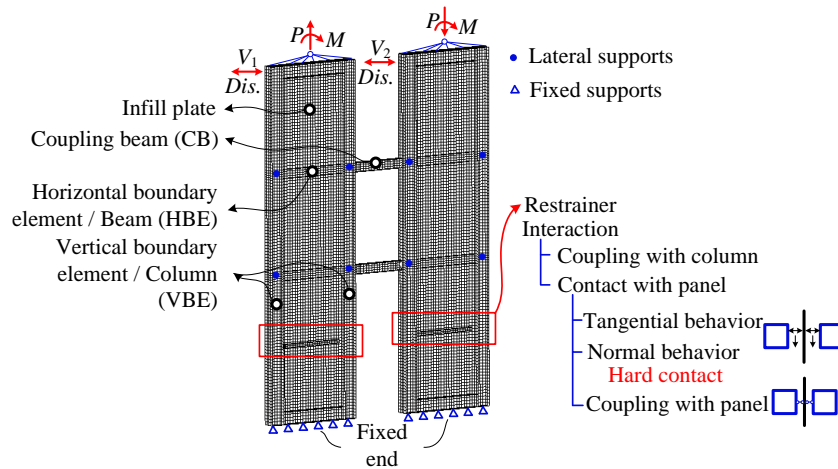


Fig.4 Numerical model

3.2 Comparison of experimental and numerical behaviors

The base shear versus lateral drift for the experimental specimens and numerical models is presented in Fig. 5. Overall, the numerical model suitably replicated the experimental global behavior, although it did exhibit less pinching response. This discrepancy is likely related to localized degradation, primarily associated with connection damage, which occurred in the experiments but was not fully captured in the models. However, the proposed model is deemed to be capable of predicting the overall load-carrying capacity and hysteretic response of SPSW-WC systems and useful for conducting additional parametric studies.

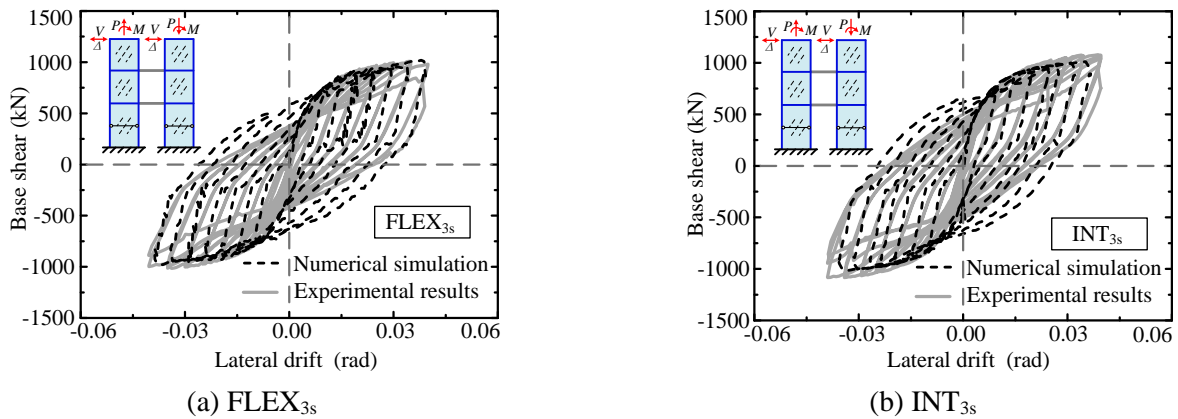


Fig.5 Comparison of tests and simulated results

The global deformation of the experimental specimens and numerical models is presented in Fig. 6. In both cases, plastic hinges formed in the RBS regions of the HBEs and at the base of the VBEs, and yielding mechanisms (flexural or shear) with large rotations developed in the coupling beams. Additionally, the numerical models captured shear buckling and tension field action of the infill plates, as well as the plastic strain accumulation in the HBEs and VBEs. The yield mechanisms of the CBs in the FLEX_{3s} and INT_{3s} specimens were replicated realistically by the models.

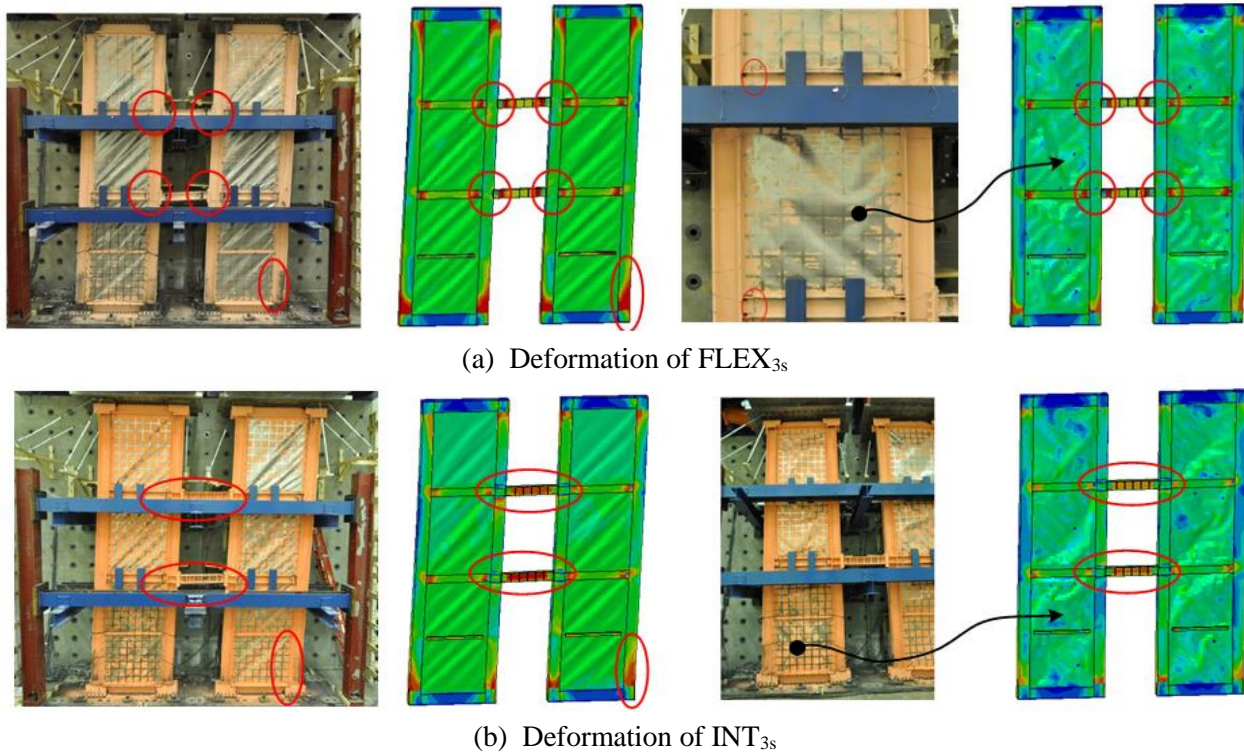


Fig. 6 Experimental specimen and numerical model global deformation

Von Mises stress and PEEQ (equivalent plastic strain, which is a measure of accumulated plastic strain) from the numerical models were used to correlate the probable fracture location and fracture tendency of the test specimens. Fig. 7 shows the observed fractures and the distribution of von Mises stress and PEEQ at the corresponding locations. At position 1 of FLEX_{3s} (Fig. 7(a)), plastic hinges were observed in the CB with substantial local buckling, corresponding to large values of von Mises stress and PEEQ in the numerical model. The connection ultimately fractured outside the region of web reinforcement (position 2 in Fig. 7(a)). Similar to the CBs, fracture occurred in the RBS regions of the HBEs (position 3 in Fig. 7(a), where repeated local

buckling was observed), which was also captured by the numerical models. At position 4 in Fig. 7(a), the whitewash had completely flaked off in the plastic hinges that formed at the bases of the VBEs. These positions were also accurately captured by the numerical model. For INT_{3s} with relatively heavier coupling beams, distributed shear yielding over the length was observed experimentally and numerically, as shown in Fig. 7(b).

In summary, the proposed three-dimensional finite element model accurately captures the global response and local behaviors of the SPSW-WC test specimens. Additionally, the numerical models provide insight into the development of stress concentrations, accumulated plastic strain and overall deformation modes. This modeling framework is a valuable tool for supplementing experimental data and carrying out further parametric analysis of the SPSW-WC configuration.

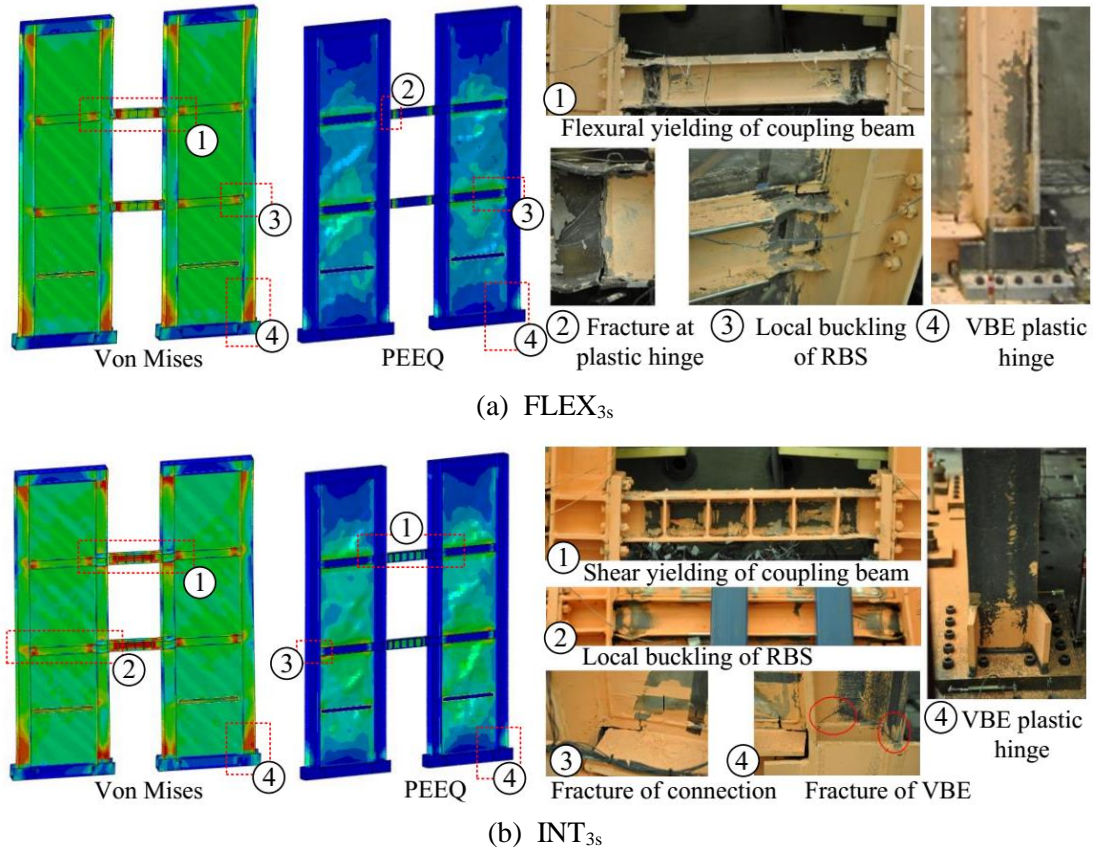


Fig. 7 Experimental and numerical localized demands

3.3 Degree of coupling and shear distribution from simulation results

One goal of the numerical model is to investigate measures that cannot be experimentally observed, such as the pier internal forces, degree of coupling, and shear distribution (between the infill plates and boundary frame). The lateral load resistance mechanism of the SPSW-WC configuration differs from the conventional SPSW due to the introduction of coupling beams [10]. An additional moment M_{coup} is formed to partially resist the overturning with opposing vertical forces P_{pier} in each pier, as shown in Fig. 8(c). This moment is given by Eq. (1). The Degree of Coupling (DC) is a well-known quantity for concrete coupled walls, and it was used by Borello and Fahnstock [11] to describe the relative interaction of two SPSW piers, defined as the ratio of coupling moments M_{coup} to the total moment M_{total} , given in Eq. (2).

$$M_{coup} = \frac{L+e}{2} \sum P_{pier} \quad (1)$$

$$DC = \frac{M_{\text{coup}}}{M_{\text{total}}} = \frac{M_{\text{coup}}}{M_{\text{coup}} + \sum M_{\text{pier}}} \quad (2)$$

The axial force P_{pier} and moment M_{pier} of each pier at the base were extracted from numerical results. The internal force values of the left and right piers were quite similar, so only data for the right pier are shown in Fig. 8(a) and (b), which are also compared with the monotonic results of the six-story models FLEX_{6s} and INT_{6s}. The axial force in the FLEX_{3s} piers, with smaller CBs, was approximately half of the INT_{3s} pier axial. However, the moment in each pier, M_{pier} , was approximately 1.5 times larger. These results were consistent with the mechanisms of SPSW-WC systems presented in references [10] and [11]. With these values, the DC at cyclic peak strength could be determined, as shown in Fig. 8(c). Because the CBs of FLEX_{3s} were lighter than INT_{3s}, the DC was smaller as expected. The minimum limit of DC for FLEX_{3s} was 0.27, compared to 0.52 for INT_{3s}, which were consistent with the analytical results [10].

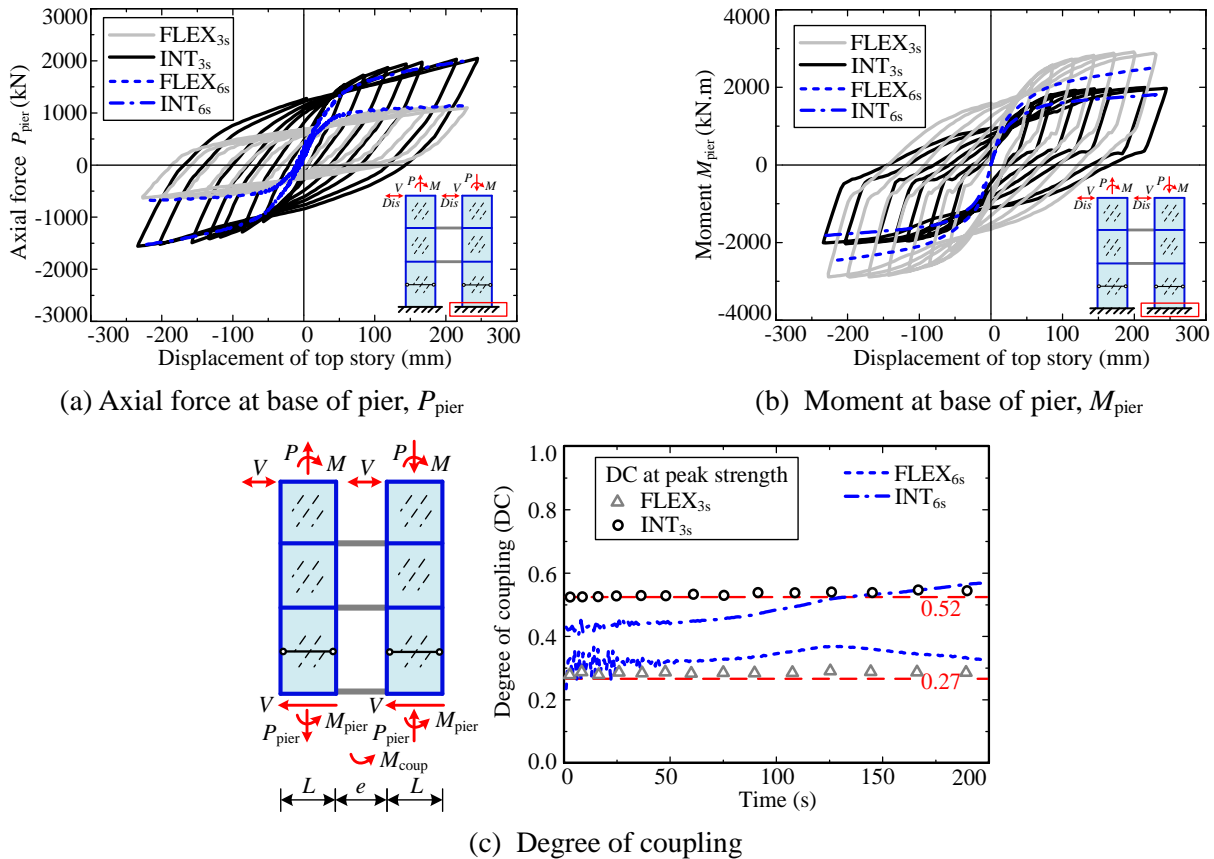


Fig.8 Pier internal forces and degree of coupling at base

The total rotation of the coupling beam $\theta_{\text{CB},i}$ was the sum of the pier rotation $\theta_{\text{pier},i}$ and the rotation of the coupling beam due to relative vertical movement of the ends $\theta_{v,i}$, as shown in Fig. 9. The positions of $v_{1,i}$ and $v_{2,i}$ were consistent with the locations of inclinometers in the tests. For FLEX_{3s}, the relative vertical rotation $\theta_{v,i}$ is similar between the experimental specimen and the numerical model (the maximum rotation was more than 0.03 rad), which was close to the story drift (more than 0.04 rad). Therefore, the coupling beam rotation was close to 0.08 rad. Due to increased coupling, the relative vertical rotations $\theta_{v,i}$ of INT_{3s} were smaller than FLEX_{3s}, leading to slightly smaller total rotation of the coupling beam $\theta_{\text{CB},i}$.

Current US SPSW design provisions [12] do not clearly prevent consideration of the boundary frame contribution to the total lateral strength, and some design examples have employed this method [1]. However, the next edition of US SPSW design provisions will require that the full design shear be resisted by the infill plate alone. To investigate the distribution of shear between the infill plate and the boundary frame, the total

shear resisted by the infill plates V_{plate} at the base was extracted from the numerical results, shown in Fig. 10(a). Because the infill plates were thin, significant pinching can be observed in the hysteretic curves, and the post-buckling strength was fully developed. The total shear resisted by the boundary frame V_{frame} at the base is shown in Fig. 10(b), and the curves are quite full. By comparing Fig. 10(a) and 10(b), it can be seen that when the tension fields of the infill plates were fully developed, the resistance of the infill plate was similar for both specimens, approximately one-half to one-third of the total shear. In the SPSW-WC configuration, frame action is intrinsically more influential than in the standard uncoupled configuration, and sharing design shear between the infill plate and boundary frame should be considered as a viable strategy, as done in the present frames [10].

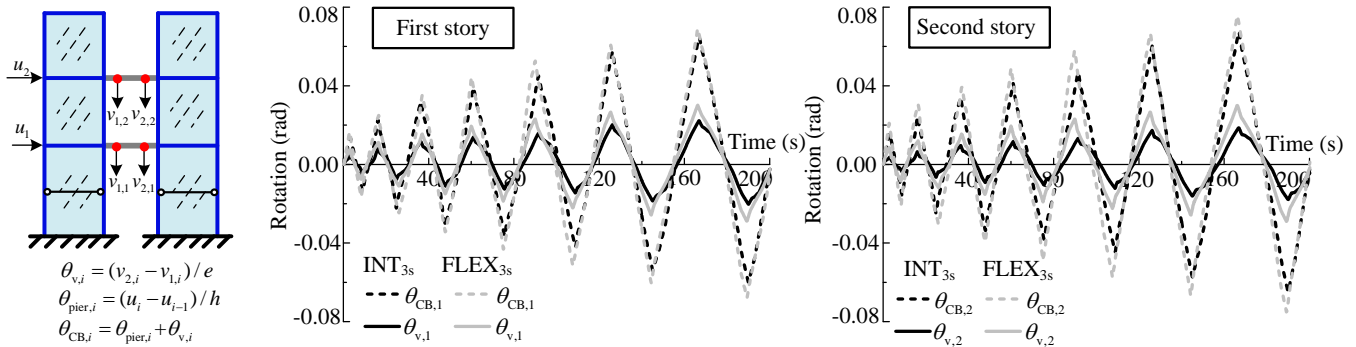


Fig. 9 Coupling beam rotation

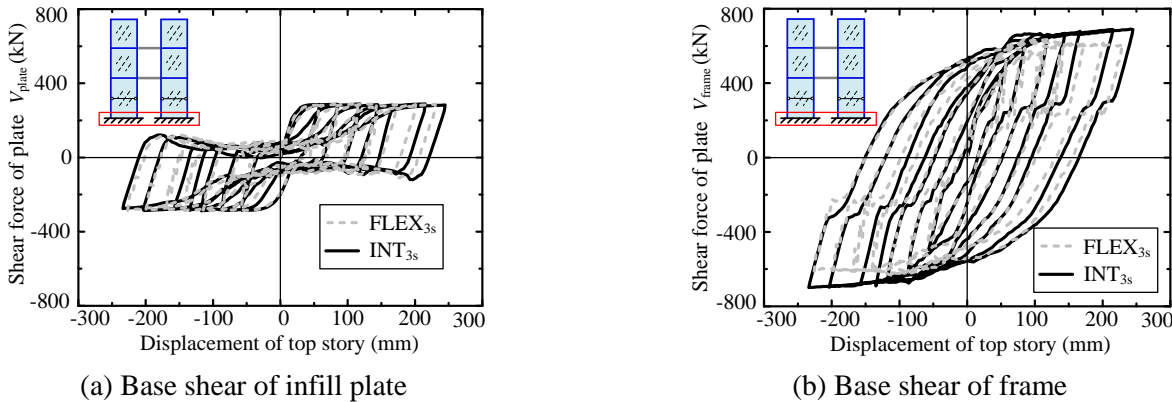
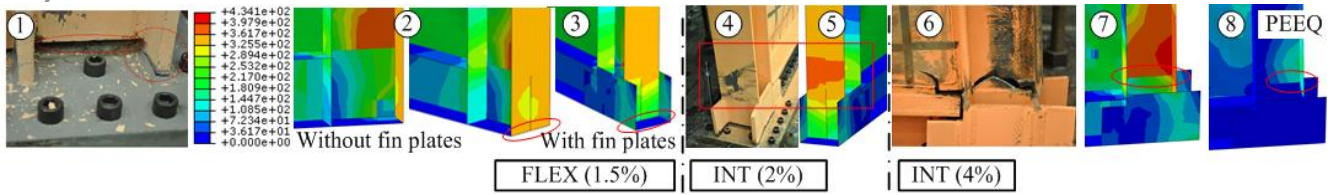


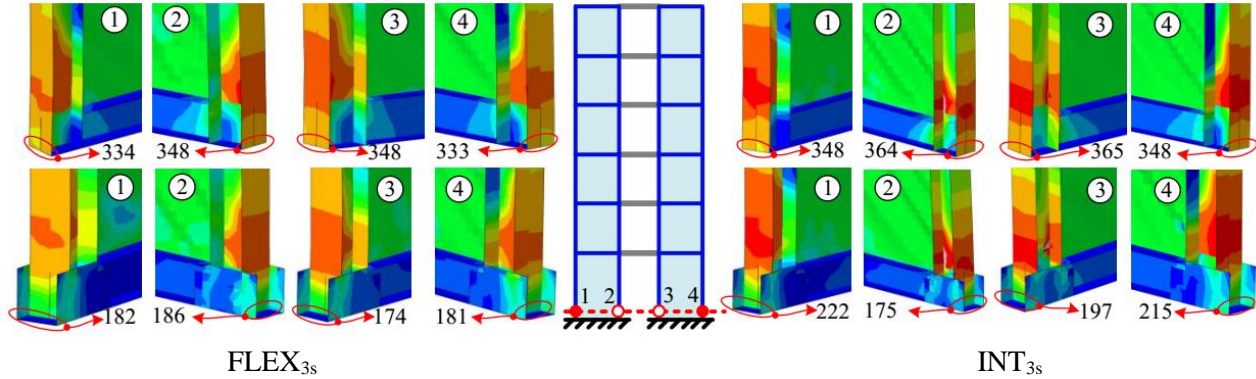
Fig.10 Base shear distribution between plate and frame

3.4 Failure analysis of VBE base connections

VBE base connections are a critical region of high demand in SPSWs, so strategies to protect these regions are important. As shown in Fig. 11(a)-1, the original FLEX_{3s} VBE base details were unstiffened, and at 1.5% drift, the VBE-to-base plate weld fractured due to excessive demand, illustrated by finite element stress contour plots in Fig. 11(a)-2. According to related material tests [13], the ductility and fatigue behaviors of weld and transition regions are much worse than the base metal. Therefore, high stresses and large plastic strains can cause brittle low-cycle fatigue failure in welded regions. After this sudden failure, the specimen was unloaded for retrofit. To reduce the localized demands in this region, fin plates were added, which successfully shifted the plastic hinge away from the welded connection, as shown in Fig. 11(a)-3. The INT_{3s} specimen was also reinforced with fin plates. As shown in Fig. 11(a)-4 and 5, the VBE base was still intact at 2% drift. Fig. 11(b) compares the von Mises stress distributions of VBE base connections with and without fin plates. The stresses exceeded the flange yield stress in the situation without fin plates, but the stresses in the situation with fin plates were much lower than yield stress (around half of yield), indicating the welded connections were still elastic. After this retrofit, at 4% drift, the VBES of INT_{3s} fractured just above the fin plates (Fig. 11(a)-6), where both von Mises and PEEQ reached the maximum values (Fig. 11(a)-7 and 8). This fracture was caused by low cycle fatigue from local buckling at the plastic hinge. In summary, reinforcement of VBE bases with fin plates is an option for avoiding brittle fracture in the welded region.



(a) Failure behaviors of VBE base for FLEX_{3s} and INT_{3s} (stress units: MPa)



(b) von Mises stress distributions of VBE base at 4% top drift angle (stress units: MPa)

Fig. 11 Localized demands at VBE base

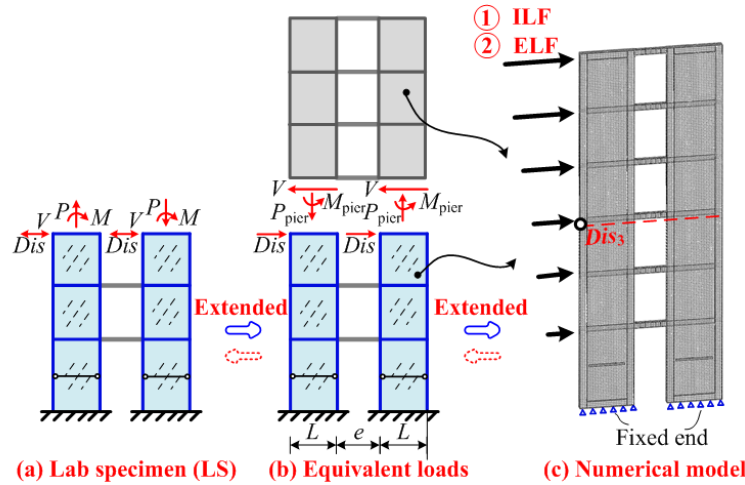


Fig. 12 Details of the reduced-scale model (FLEX_{6s} and INT_{6s})

4. Numerical analysis of six-story reduced-scale models

4.1 Description of the six-story reduced-scale models

The lab three-story specimens (FLEX_{3s} and INT_{3s}) were designed to represent the bottom three stories of a six-story structure (Fig. 1 and Fig. 12(a)). To compare the behaviors of the lab specimens with the six-story reduced-scale models, the numerical models were extended to six stories, as show in Fig. 12(b) and (c). The section dimensions of the six-story reduced-scale specimens (FLEX_{6s} and INT_{6s}) were the same as the lab specimens (FLEX_{3s} and INT_{3s}). The pushover analyses of these two specimens were carried out under two force profiles: the equivalent lateral force (ELF) and inelastic lateral force (ILF). The internal forces at the third floor of the reduced-scale models (FLEX_{6s} and INT_{6s}) were extracted (Fig. 12(b)), including shear forces, pier axial forces P_{pier} and pier bending moments M_{pier} , which were then compared with the imposed loads from the tests to verify the equivalence and accuracy of the boundary conditions for the lab specimens.

4.2 Comparison of pushover analysis

Fig. 13 compares the base shear versus drift at the third floor of the reduced-scale models under two loading patterns (ELF_{6s} and ILF_{6s}) with the three-story models and the experimental response. As expected, the variation in response for the two load profiles is minor, although strengthening of the upper stories that results from designing for the ILF profile produces important differences in dynamic response [10]. The responses of the reduced-scale models (ELF_{6s} and ILF_{6s}) were close to the experimental results and three-story models (FLEX_{3s} and INT_{3s}), confirming that the three-story test specimens capture the behaviors of the six-story structures.

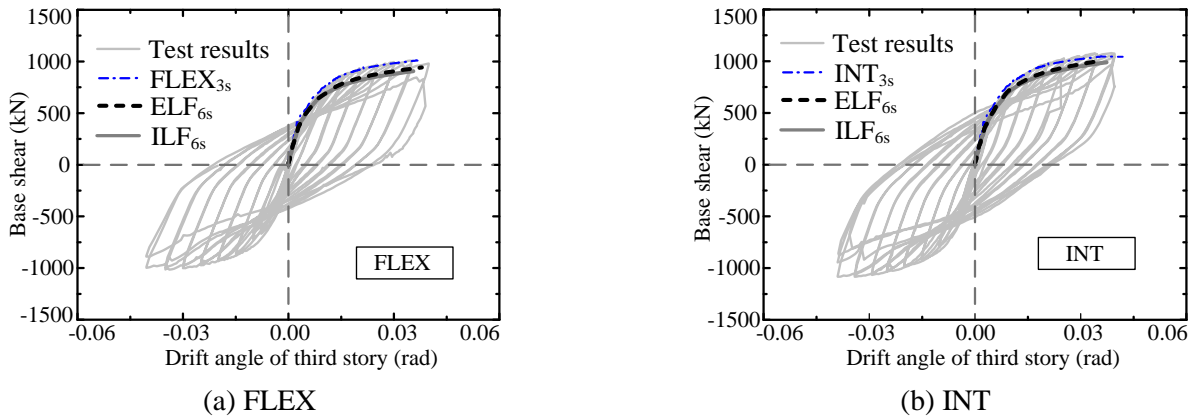
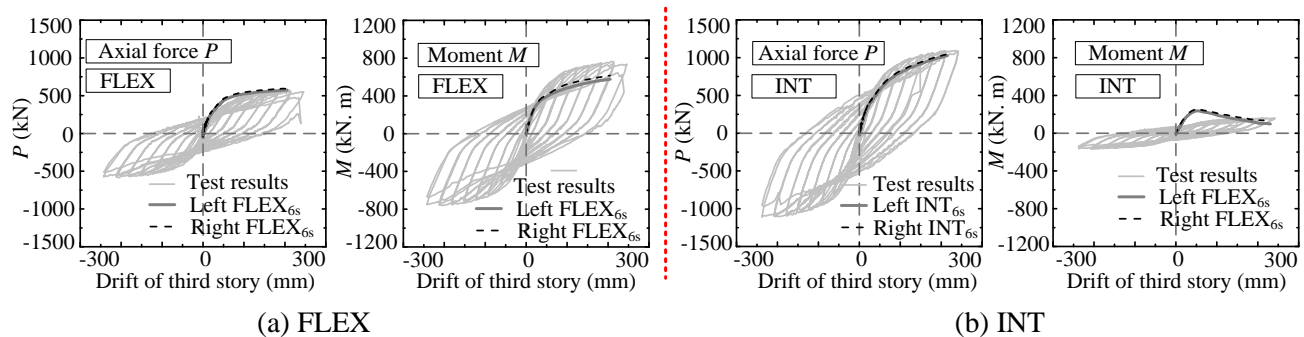


Fig. 13 Global response of three-story models, six-story models, and experimental specimens

Since results for the two loading patterns were similar, the ILF will be used for discussion. These internal forces were also compared with the applied forces for the tests, shown in Fig. 14(a) and (b). The extracted internal axial forces P_{pier} at the third story were consistent with the cyclic skeleton curves of the applied axial forces in the experimental specimen. However, the bending moments M_{pier} of FLEX_{6s} were smaller than the experimental moments and the INT_{6s} were larger. These differences are related to the simplified modeling of the upper three stories for determining the moments that were applied experimentally. However, these local differences have little influence on the global behavior. Therefore, the use of the simplified experimental boundary conditions is justified and consistent with a six-story building.

Based on the extracted internal forces (M_{pier} and P_{pier}) of the six-story reduced-scale models (Fig. 14(a) and (b)) at the third floor, the DC at the third level is obtained from Eq. (2) and plotted (Fig. 14(c)). At this level, the DC targets of FLEX_{3s} and INT_{3s} in the tests were 0.5 and 0.9, respectively [4]. To further investigate the DC development during the loading process, the axial forces P_{pier} and bending moments M_{pier} of each pier at the base of the six-story models subjected to ILF (FLEX_{6s} and INT_{6s}) were also extracted, and compared with the numerical results of the three-story models (FLEX_{3s} and INT_{3s}), as shown in Fig. 8(a) and (b). Similar to the results at the third level, the extracted axial forces P_{pier} of the six-story model at the base were consistent with the six-story models, while the bending moments M_{pier} were slightly smaller. DC at the base is plotted in Fig. 8(c) and the trends are consistent with the analytical results for full-scale models of FLEX and INT walls presented in reference [10].



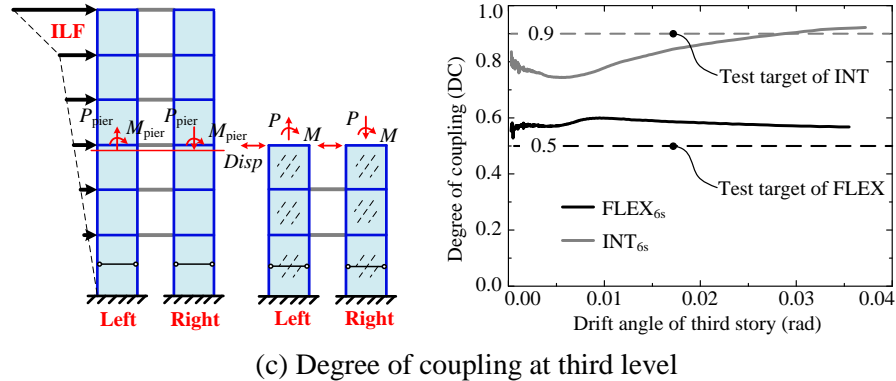


Fig. 14 Internal forces and degree of coupling of the six-story numerical models and experimental specimens.

Fig. 15 qualitatively compares the failure modes of the six-story models, three-story models and experimental specimens. The deformations of the bottom three stories of the six-story models were consistent with the three-story models and experimental specimens, including the buckling and tension field yielding of the infill plates, plastic hinging in the RBS regions of HBEs, VBE base plastic hinging, and coupling beam yielding (flexural for FLEX and shear for INT). The comparison also indicates that the three-story test specimens well represent the behaviors of the whole six-story structure.

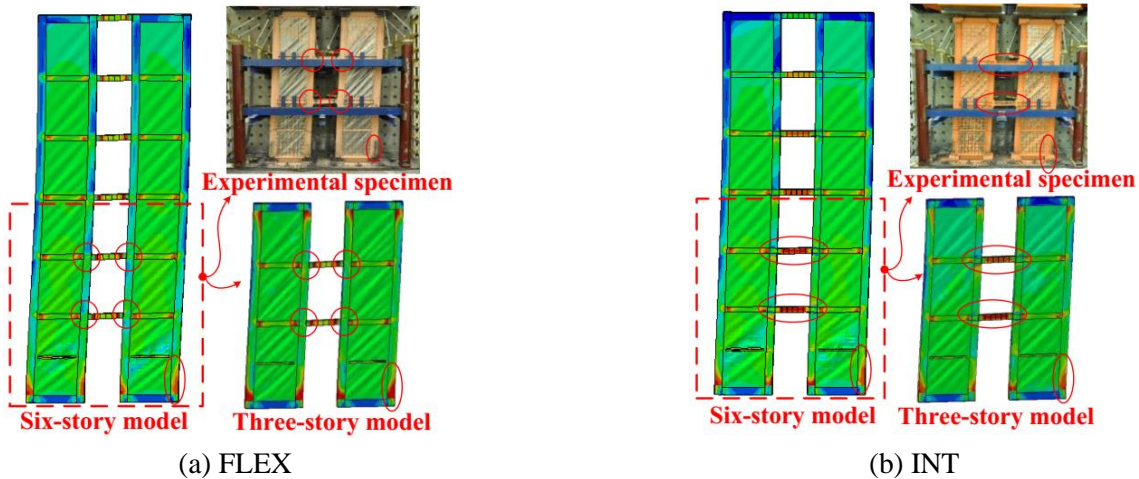


Fig.15 Comparison of failure mechanisms of six-story models, three-story models, and experimental specimens.

5. Summary

(1) The proposed finite element modeling approach not only captured experimental behaviors of two SPSW-WC specimens – including ultimate capacity, overall cyclic response and local demands and distribution of damage – but also presented additional characterization of response that could not be measured in the experimental test program. The modeling method provides a valuable tool for carrying out further parametric studies of other SPSW-WC configurations.

(2) Based on the results from the verified numerical models, several aspects of the test specimen behavior that were not measured experimentally were studied. a) At the base, the minimum degree of coupling was 0.27 for FLEX and 0.52 for INT, and these values are consistent with the analytical predictions. b) The maximum coupling beam rotation was close to 0.08 rad for FLEX, with INT experiencing slightly smaller coupling beam rotations. This level of coupling beam rotation is roughly double the top drift of 0.04 rad and illustrates the robustness of coupling beam behavior for large inelastic deformations. c) The proportion of the base shear resisted by the infill plates ranged from one-third to one-half of the total, demonstrating the significance of



considering the boundary frame contribution in proportioning the SPSW-WC configuration. For the two designs considered, the ultimate base shear capacity was very similar, but INT was lighter than FLEX owing to the higher degree of coupling and the associated boundary frame contribution. d) Reinforcement of VBE bases with fin stiffener plates is an effective method to protect the welded connection to the base plate and move the plastic hinge away from the region that is most vulnerable.

(3) According to the comparisons of results for the six-story models, the three-story models and the experimental specimens, the three-story specimens that were tested with a hybrid simulation technique successfully represented the behavior of the six-story structures. The equivalence and accuracy of the experimentally imposed loading and boundary conditions were validated.

Acknowledgements

Funding for the tests described in this paper was provided by the United States National Science Foundation (Grant No. CMMI-0830294). The first author of this paper was supported by a Chinese National Natural Science Foundation Grant (No. 51408031). All opinions, findings, and conclusions are those of the authors.

References

- [1] Sabelli R, Bruneau M (2006): AISC Design Guide 20 - Steel Plate Shear Walls, *American Institute of Steel Construction*.
- [2] ENR (2010): Last Piece of L.A. Live Opens – Ritz-Carlton, Los Angeles, *Engineering News Record*, <http://www.enr.com/articles/19128-last-piece-of-l-a-live-opens-ritz-carlton-los-angeles> (accessed March 28, 2016).
- [3] Berman J W (2011): Seismic behavior of code designed steel plate shear walls. *Engineering Structures*, **33**(1), 230–244.
- [4] Borello D J (2014): Behavior and large-scale experimental testing of steel plates shear walls with coupling. *PhD thesis*, University of Illinois at Urbana-Champaign, Illinois, USA.
- [5] Li C H, Tsai K C, Chang J T, Lin C H, Chen J C, Lin T H, Chen P C (2012): Cyclic test of a coupled steel plate shear wall substructure. *Earthquake Engineering and Structural Dynamics*, **41**(9), 1277–1299.
- [6] Borello D J, Quinonez A A, Fahnestock L A (2014): Shear plate shear walls with coupling in high-seismic regions. *In Proceedings of the 10th National Conference in Earthquake Engineering*, Earthquake Engineering Research Institute, Anchorage, AK.
- [7] Dubina D, Dinu F (2014): Experimental evaluation of dual frame structures with thin-walled steel panels. *Thin-walled Structures*, **78**, 57-69.
- [8] Dusicka P, Lewis G (2010): Investigation of Replaceable Sacrificial Steel Links. *In Proceedings of the 9th US National and 10th Canadian Conference on Earthquake Engineering. 9th US National and 10th Canadian Conference on Earthquake Engineering*, Toronto, Ontario, Canada.
- [9] ABAQUS (2010): Analysis user's manual I_V. Version 6.10. USA: ABAQUS, Inc., Dassault Systèmes.
- [10] Borello D J, Fahnestock L A (2013): Seismic design and analysis of steel plate shear walls with coupling. *Journal of Structural Engineering*, **139**, 1263-1273.
- [11] Borello D J, Fahnestock L A (2012): Behavior and mechanisms of steel plate shear walls with coupling. *Journal of Constructional Steel Research*, **74**, 8-16.
- [12] AISC (2010): Seismic provisions for structural steel buildings. ANSI/AISC 341-10. *American Institute of Steel Construction*.
- [13] Shi G, Wang M, Wang Y Q, Wang F (2013): Cyclic behavior of 460MPa high strength structural steel and welded connection under earthquake loading. *Advances in Structural Engineering*, **16**(3), 451-466.